

Full paper

## Rational design of porous structures via molecular layer deposition as an effective stabilizer for enhancing Pt ORR performance

Lei Zhang<sup>a</sup>, Yang Zhao<sup>a</sup>, Mohammad Norouzi Banis<sup>a</sup>, Keegan Adair<sup>a</sup>, Zhongxin Song<sup>a</sup>, Lijun Yang<sup>b</sup>, Matthew Markiewicz<sup>b</sup>, Junjie Li<sup>a</sup>, Sizhe Wang<sup>a</sup>, Ruying Li<sup>a</sup>, Siyu Ye<sup>b</sup>, Xueliang Sun<sup>a,\*</sup>

<sup>a</sup> Department of Mechanical and Materials Engineering, The University of Western Ontario, London, ON, N6A 5B9, Canada

<sup>b</sup> Ballard Power Systems Inc., 9000 Glenlyon Parkway, Burnaby, BC, V5J 5J8, Canada

## ARTICLE INFO

## Keywords:

Platinum  
Molecular layer deposition  
X-ray adsorption spectrum  
Fuel cells  
Oxygen reduction reaction

## ABSTRACT

Pt-based catalysts are widely applied in fuel cells as key components of both anode and cathode. However, commercial Pt/C catalysts with Pt nanoparticles dispersed on carbon support exhibit poor durability due to the Ostwald ripening effect, detachment and agglomeration of Pt nanoparticles during fuel cell operation. Herein, we demonstrate for the first time the application of molecular layer deposition (MLD) to stabilize Pt catalysts. By atomic layer deposition (ALD) of Pt particles on MLD-derived interlayer, the Pt catalysts show significantly enhanced oxygen reduction reaction (ORR) activity and durability compared to that without the MLD interlayer. The MLD-derived surfaces with enriched pores are helpful for anchoring the Pt nanoparticles and to avoid agglomeration or detachment from the surface sites. In addition, X-ray adsorption spectroscopy (XAS) results show that the deposition of Pt on the MLD-derived interlayer caused the electron transfer from Pt to substrates, which results in a decrease in the number of electrons in the d orbital of Pt. In addition, the extended X-ray absorption fine structure (EXAFS) result indicates that Pt–Pt bond distance is shortened by the deposition on the MLD-derived NCNT, which leads to the enhanced activity of Pt catalysts. This work provided a novel route for stabilizing Pt catalysts through MLD technique.

### 1. Introduction

Pt-based catalysts are widely applied in proton exchange membrane fuel cells (PEMFCs) as key components of both anode and cathode due to their effective catalytic properties in both hydrogen oxidation and oxygen reduction reactions [1–5]. However, commercial Pt/C catalysts in the PEMFCs exhibit low durability during operation under severe conditions, such as low pH (< 1), high oxygen concentration, high humidity, and at varied potentials. The significant drop in activity of Pt/C catalysts was caused by the Ostwald ripening effect (dissolution of the cationic Pt species from the small Pt metal particles and re-deposition on large metal particles), detachment of Pt nanoparticles (NPs) from the support, and Pt NPs agglomeration [6–10]. Hence, it is of great importance to develop effective routes to stabilize Pt catalysts and prevent the activity loss during fuel cell operation.

Depositing a thin layer of metal oxide on top of the supported metal NPs has demonstrated as an attractive way to inhibit the migration of metal NPs and thus enhance their stability. Up till now, several types of inorganic oxides have been developed, such as zirconia [11], silica [12–14], or tin oxide [15]. However, it is a great challenge to precisely

control the thickness of porous overlayers. In the past few years, atomic layer deposition (ALD) of metal oxides on metal NPs have attracted significant attention due to its unique advantages in precise control of thickness and size of the metal oxide layer. For example, porous alumina layers were coated on Pd NPs by precisely control alumina layer thickness based on sequential and self-limiting surface reactions [16,17]. Cheng and co-workers stabilized Pt catalysts in zirconia nanocages by area-selective ALD [18]. The prepared Pt catalyst encapsulated in zirconia nanocages showed very high stability and activity towards oxygen reduction.

Recently, molecular layer deposition (MLD), as an analogue of ALD, has been employed to produce inorganic–organic hybrid thin films with many advantages [19–23]. In comparison to inorganic metal oxide deposition through ALD, the properties of inorganic–organic hybrid coatings can be easily modified by tuning the organic groups. Among various types of inorganic–organic hybrid coatings, alucone have been widely used as an effective material for interlayer development and improving the stability of catalysts [24–27]. For instance, our group has demonstrated the use of MLD alucone as a coating material to improve the electrochemical performance of carbon/sulfur cathodes in Li–S

\* Corresponding author.

E-mail address: [xsun@eng.uwo.ca](mailto:xsun@eng.uwo.ca) (X. Sun).

<https://doi.org/10.1016/j.nanoen.2019.03.033>

Received 18 January 2019; Received in revised form 28 February 2019; Accepted 9 March 2019

Available online 13 March 2019

2211-2855/ © 2019 Published by Elsevier Ltd.

batteries and sodium metal anodes [24,25]. Alucone has also been applied for the stabilization of Pt NPs. Weimer et al. found that alucone-coated Pt NPs showed much more stable properties to calcination in air at 800 °C [26,27]. Unfortunately, the catalysts with fully covered MLD coating showed an expense of significantly lowered catalytic activity as compared to that of the supported Pt NPs. By using trimethylaluminum (TMA) and glycerol (GLY) as the precursors, sequential MLD reactions will produce a high degree of cross-linking between the polymer chains, which strengthens the alucone films and lead to higher fracture toughness. The growing organic-inorganic film with abundant pores will be helpful for building up a 3D porous network during the MLD process [20,23]. It should be pointed that the thin MLD coating cannot be directly applied in protection of Pt NPs for fuel cell reactions due to its poor conductivity. To solve the low conductivity issue of alucone coating, the MLD layer can be annealed to form an MLD-derived carbon-based interlayer. After annealing, the as-prepared MLD-derived carbon-based interlayer might have porous structure, which is helpful for anchoring the Pt catalysts and to avoid agglomeration or detachment from the surface sites.

Herein, for the first time, we demonstrate the application of an annealed MLD interlayer for Pt catalysts deposition. The MLD-derived layer was fabricated by using trimethylaluminum and glycerol (named as TMA-GLY) on nitrogen-doped carbon nanotubes (NCNT), followed by calcination to create porous structures. Subsequently, the ALD process was carried out to deposit Pt NPs on the MLD-NCNTs support and the as-prepared catalysts are denoted as NCNT-MLD-Pt. The enriched pores are helpful for anchoring the Pt nanoparticles to avoid agglomeration and detachment. Compared to NCNT-Pt catalysts, the NCNT-MLD-Pt shows significantly enhanced ORR activity and durability. In addition, the enhanced mechanism was carefully investigated by X-ray absorption spectroscopy (XAS).

## 2. Experimental section

### 2.1. Preparation of TMA-GLY MLD layer on NCNT

NCNTs with an average diameter of 100 nm were prepared by ultrasonic spray pyrolysis as outlined previously [28]. Molecular layer deposition (MLD) of TMA-GLY coatings were conducted in a Gemstar-8 ALD system (Arradance, USA) directly connected with argon-filled glove box. The TMA-GLY films was directly deposited on the NCNT at 150 °C by alternatively introducing trimethylaluminum (TMA) and glycerol (GLY) as precursors. TMA and glycerol (GLY) were introduced into the chamber using a program of 0.1 s/40 s/1 s/60 s. GLY was kept in an external reservoir set to 140 °C while the oxidizing manifold was heated to 150 °C. After the MLD process, the NCNT-MLD samples were heated in air at 400 °C for 3 h to obtain MLD-derived porous structure.

### 2.2. ALD synthesis of Pt catalysts on NCNT with MLD-derived porous structure

Pt was deposited on the NCNT with MLD-derived porous structure by ALD (Savannah 100, Cambridge Nanotechnology Inc., USA) using trimethyl(methylcyclopentadienyl)-platinum (IV) (MeCpPtMe<sub>3</sub>) and O<sub>2</sub> as precursors. High-purity N<sub>2</sub> (99.9995%) was used as both a purging gas and carrier gas. The deposition temperature was 230 °C, while the container for MeCpPtMe<sub>3</sub> was kept at 65 °C to provide a steady-state flux of Pt to the reactor. For each ALD cycle, 1 s of the MeCpPtMe<sub>3</sub> pulse and 5 s of the O<sub>2</sub> pulse were separated by a 20 s N<sub>2</sub> purge. The Pt particles on NCNT with MLD-derived porous structure were obtained after several ALD cycles. With different Pt ALD cycles on NCNT-MLD, the loading amount of Pt on NCNT-MLD is 4.6%, 10.7 and 15.3% for 10, 20 and 30 cycles, respectively. Herein, we used NCNT-MLD-Pt with 30 cycles Pt ALD sample for further study. The Pt catalysts on NCNT with different cycle numbers of 10, 30 and 50 MLD TMA-GLY coating are named as NCNT-10MLD-Pt, NCNT-30MLD-Pt and NCNT-50MLD-Pt,

respectively.

### 2.3. Electrochemical measurements

The electrochemical measurements were performed using a glassy carbon rotating-disk electrode (Pine Instruments) as the working electrode with a platinum wire and a reversible hydrogen electrode (RHE) as the counter and reference electrodes, respectively. An ink for the electrochemical measurement was prepared by adding 3 mg of the catalysts into a mixture of DI water (1.6 mL), isopropanol (0.4 mL, Sigma-Aldrich), and Nafion (5% solution, Sigma-Aldrich, 40 μL), followed by sonication for 10 min. A working electrode was prepared by loading the ink (10 μL) on the glassy carbon electrode. The cyclic voltammograms (CVs) were measured in a N<sub>2</sub>-saturated electrolyte by cycling between 0.05 and 1.1 V<sub>RHE</sub> at a sweep rate of 0.05 V s<sup>-1</sup>. The ORR test was carried out in an O<sub>2</sub>-saturated electrolyte with a scan rate of 0.01 V s<sup>-1</sup> and a rotation speed of 1,600 rpm.

### 2.4. Instrumentation

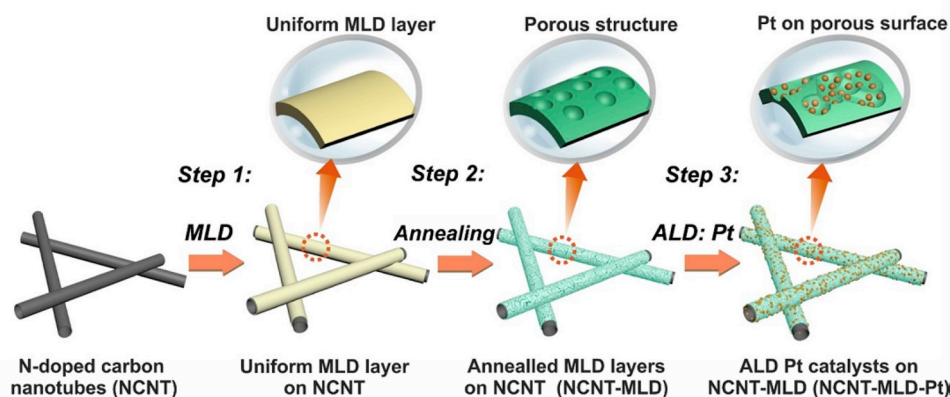
The SEM images were taken by scanning electron microscopy (SEM, S-4800). TEM samples were prepared by drop casting an ultrasonicated solution of dilute high-performance liquid chromatography grade methanol solution with the sample of interest onto a lacey carbon grid. The TEM images, high-resolution TEM (HRTEM) and high-angle annular dark-field scanning transmission electron microscopy (HAADF-STEM) were taken on the Jeol 2010F TEM. The Pt loading amount on NCNT and NCNT-MLD was determined by inductively coupled plasma-optical emission spectroscopy (ICP-OES).

### 2.5. X-ray absorption spectroscopy

XANES measurements of the Pt L3-edge were conducted on the 061D superconducting wiggler at the hard X-ray microanalysis beamline at the Canadian Light Source. Each sample spectra was collected using fluorescence yield mode with a solid-state detector. High purity Pt metal foil was collected in transmission mode for comparison and monochromatic energy calibration. The obtained XAS data were analyzed using Athena software. The extracted EXAFS data was weighted by k<sup>3</sup> to obtain the magnitude plots of the EXAFS spectra in radial space. The data was fitted using Artemis software.

## 3. Results and discussion

**Scheme 1** shows the main steps for the preparation of NCNT-MLD-Pt catalysts on NCNT through MLD and ALD methods. NCNTs with an average diameter of 100 nm were prepared by ultrasonic spray pyrolysis as outlined previously [28]. The MLD TMA-GLY thin film was deposited on the NCNTs using sequential exposures of TMA and glycerol at 150 °C in a glovebox-integrated ALD tool. As shown in **Fig. S1**, 30 cycles of deposition was conducted on NCNT, indicating a uniform and conformal MLD process. To improve the conductivity and surface area of the MLD interlayer, we annealed the NCNT-MLD material in air at 400 °C for 3 h. The scanning electron microscope (SEM) and transmission electron microscope (TEM) image show that the surface of NCNT become rough, indicating the decomposition of the TMA-GLY layer (**Fig. 1a** and **b**). The high-resolution TEM image shows that the MLD-derived interlayer exhibited amorphous structure (**Fig. 1c**). The porous and rough surface of the NCNTs can be clearly observed by scanning transmission electron microscope (STEM) images (**Fig. 1d**). The porous structure cause by the TMA-GLY MLD layer is expected to lead to a higher surface area on the NCNTs surface. The surface area and pore volume of the catalysts were tested by nitrogen absorption/desorption isotherms. The specific surface area and pore size distribution of NCNT and NCNT-MLD as well as textural properties are shown in **Fig. 1e**. The surface area of NCNT after the deposition of the annealed



**Scheme 1.** A schematic illustration showing the preparation process of the NCNT-MLD-Pt catalyst.

MLD layer is increased from 52.8 to 90.9 m<sup>2</sup>/g. As shown in Fig. 1f, the NCNT-MLD exhibit greater porosity in the 5–10 nm range. This result suggests the generation of mesopores on the MLD layer after the annealing process. In addition, there is an increase in pore volume from 0.086 cm<sup>3</sup> g<sup>-1</sup> to 0.173 cm<sup>3</sup> g<sup>-1</sup> observed for NCNT and NCNT-MLD, respectively. Given the results presented by SEM, STEM and N<sub>2</sub> adsorption/desorption isotherms, the porous structures are successfully prepared through the MLD derived method.

Pt particles were deposited onto the surface of MLD-modified NCNT through an ALD process by using trimethyl(methylcyclopentadienyl)platinum (IV) (MeCpPtMe<sub>3</sub>) and O<sub>2</sub> as the precursor, and nitrogen (99.9995%) as purge gas. As shown in Fig. 2a, the SEM images indicated that Pt NPs are successfully deposited onto the substrates after 30 cycles Pt ALD. The as-prepared NCNT-MLD-Pt catalyst has also been characterized by TEM. As shown in the typical low-resolution TEM image, the Pt NPs are well dispersed on MLD-modified NCNT substrates (Fig. 2b). The high-resolution TEM image clearly shows uniform Pt particles formed (Fig. 2c). The average size of Pt particles is 4.8 nm (Fig. S2). The periodic fringe spaces are confirmed to be 0.22 nm, which agree well with the *d* values for the (111) of Pt. It should be pointed that we did not observe the crystal lattice of alumina, indicating the formation of amorphous Al compounds. The energy-dispersive X-Ray spectroscopy (EDS) mapping profiles shown in Fig. 2d clearly reveal the

well distribution of C, Al and Pt elements on the whole NCNT.

Herein, we use the oxygen reduction reaction (ORR) as a model system to characterize the catalytic activities of the NCNT-MLD-Pt catalysts. As comparison, we deposited Pt particles with the size of 4.2 nm (Fig. S3 and S4) onto NCNTs without MLD coating (denoted hereafter as NCNT-Pt). The loading amount of Pt on NCNT-MLD and NCNT and was 15.3 and 14.6%, respectively, according to the ICP-OES results. Cyclic voltammograms (CV) of NCNT-MLD-Pt, NCNT-Pt and commercial Pt/C (40%) catalysts were recorded in 0.10 M aqueous HClO<sub>4</sub> at a scanning rate of 50 mVs<sup>-1</sup> (Fig. 3a). The smaller double layer capacitance on NCNT-MLD-Pt was due to the formation of MLD-derived pore structures. The ECSAs were determined by the charges associated with the desorption peaks of the underpotentially deposited hydrogen as shown in Fig. 3a. The specific ECSAs were calculated to be 49.3 and 43.3 m<sup>2</sup>/g<sub>Pt</sub> for the NCNT-MLD-Pt and NCNT-Pt catalysts, respectively. With a MLD-derived interlayer on NCNT, the ECSA of the NCNT-MLD-Pt catalysts were still comparable to that of the NCNT-Pt catalyst.

We then compared the ORR current densities of the NCNT-MLD-Pt, NCNT-Pt and commercial Pt/C catalysts at room temperature in an O<sub>2</sub>-saturated aqueous HClO<sub>4</sub> solution (0.1 M) with a rotation speed of 1,600 rpm for the working electrode. The ORR curve showed that the NCNT-MLD-Pt exhibited much better activity than NCNT-Pt and

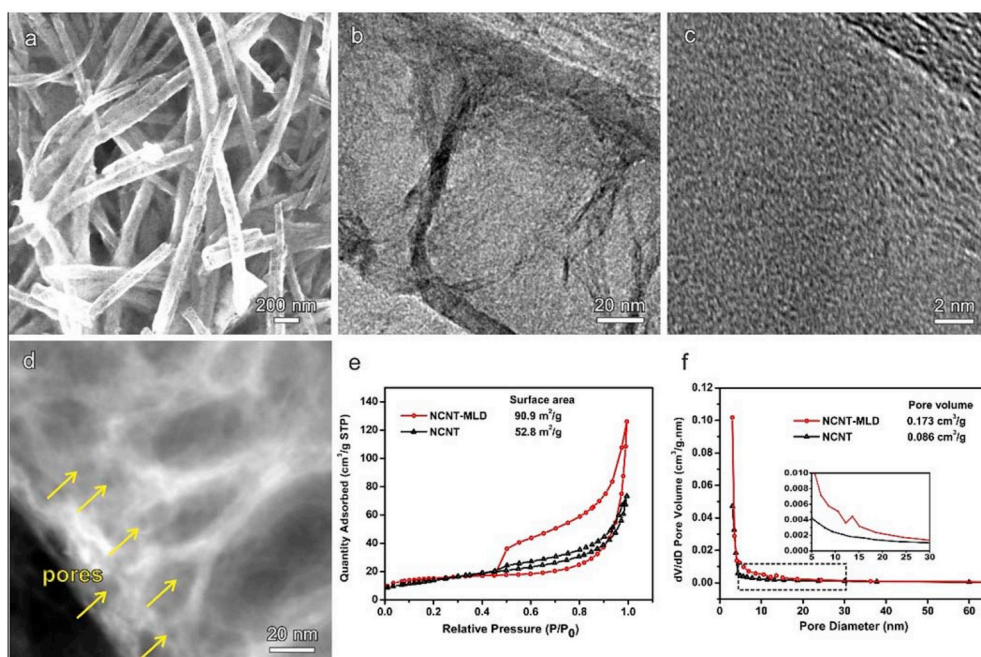


**Fig. 1.** (a, b) Typical SEM and TEM images of the NCNT-30MLD sample after annealing at 400 °C for 3 h. (c) HR-TEM image of the annealed NCNT-30MLD showing the formation of amorphous MLD layer. (d) STEM image of the annealed NCNT-30MLD showing the porous structure on NCNTs. (e) N<sub>2</sub> adsorption-desorption isotherms and (f) pore size distribution data obtained by the Barrett-Joyner-Halenda (BJH) method of NCNT and annealed NCNT-30MLD sample.

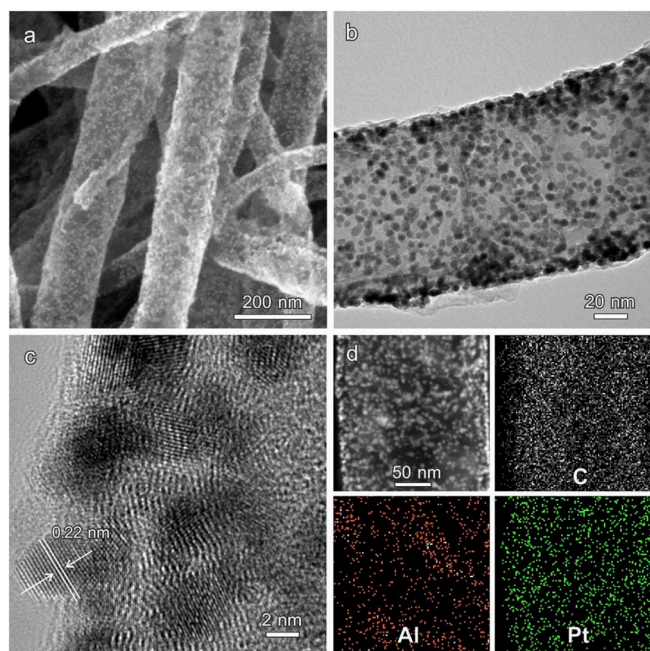


**Fig. 2.** (a) Low resolution SEM image of NCNT-MLD-Pt catalyst. (b) Typical TEM image of NCNT-MLD-Pt catalyst. (c) HR-TEM image of NCNT-MLD-Pt catalyst showing the formation of Pt nanoparticles on NCNTs. (d) HAADF-STEM image and corresponding HAADF-STEM-EDS elemental mapping of one NCNT-MLD-Pt catalyst.

commercial Pt/C (Fig. 3b). In order to compare the activity for these three catalysts, we calculated the kinetic current density ( $j_k$ ) for ORR using the Koutecky-Levich equation [29] and normalized the kinetic current to the ECSA for specific activity (Fig. 3c) and Pt loading mass for mass activity (Fig. 3d). To quantitatively compare their performance for ORR, we took the values of both specific and mass activities at 0.9

$V_{\text{RHE}}$ . As shown in Fig. 3c, the NCNT-MLD-Pt catalyst exhibited greatly improved specific activity, with  $j_k$ , specific values of  $1.34 \text{ mA/cm}^2$ , which was more than 2 times greater than that of the NCNT-Pt catalyst ( $0.61 \text{ mA/cm}^2$ ) and Pt/C ( $0.64 \text{ mA/cm}^2$ ), respectively. In addition, the NCNT-MLD-Pt catalyst also exhibited improved mass activity relative to NCNT-Pt. The mass activity at 0.9 V was  $0.66 \text{ A/mg}_{\text{Pt}}$ , which was 2.4 times higher than that of the NCNT-Pt catalyst ( $0.27 \text{ A/mg}_{\text{Pt}}$ ).

To understand the enhanced mechanism for NCNT-MLD-Pt, we utilized X-ray absorption near edge structure (XANES) and extended X-ray absorption fine structure (EXAFS) spectra to understand the electric structure of NCNT-MLD-Pt and NCNT-Pt catalyst. Fig. 4a shows the normalized XANES spectra at Pt  $L_{3\text{-edge}}$ . The threshold energy  $E_0$  is slightly negatively shifted for the NCNT-MLD-Pt and NCNT-Pt catalysts compared with Pt foil, indicating the formation of metallic Pt on both NCNT-MLD and NCNT surfaces (Table 1). In addition, the white line (WL) peak of NCNT-MLD-Pt appear to be more intense than that of Pt foil and NCNT-Pt. It has been shown that the area under the WL of the  $L_{3\text{-edge}}$  of the Pt metal is directly related to the unoccupied density of states of the Pt 5d orbitals [30,31]. An increase in the WL intensity indicate the pronounced electron transfer from Pt to substrates, which resulted in a decrease in the number of electrons in the d orbital of Pt and accounts for the excellent catalytic activity of the catalysts [30–32].

Furthermore, to study the local atomic structure of Pt, the EXAFS region of the XAS was studied. The Fourier transforms of the EXAFS region for different samples were plotted in Fig. 4b. The peak at  $2.6 \text{ \AA}$  is associated with the Pt–Pt bond, which is significant in the Pt foil, NCNT-MLD-Pt and NCNT-Pt catalyst spectra. The different EXAFS spectrum for NCNT-MLD-Pt and NCNT-Pt indicated that the Pt NPs on different substrate would cause the different Pt–Pt bond distance. The peaks are fitted to quantitatively obtain the coordination number (CN) and bonding length of Pt–Pt (Fig. 4c–e). As shown in Table 1, the Pt–Pt for the NCNT-MLD-Pt and NCNT-Pt have the much lower CN (6.05 and 5.82) relative to Pt foil (12) indicating the presence of small Pt nanoparticles on the substrates. In addition, we found the bonding distance of Pt–Pt for the NCNT-MLD decreased to 2.63, which is much lower than that of Pt foil (2.76). This result indicated that Pt–Pt bond distance

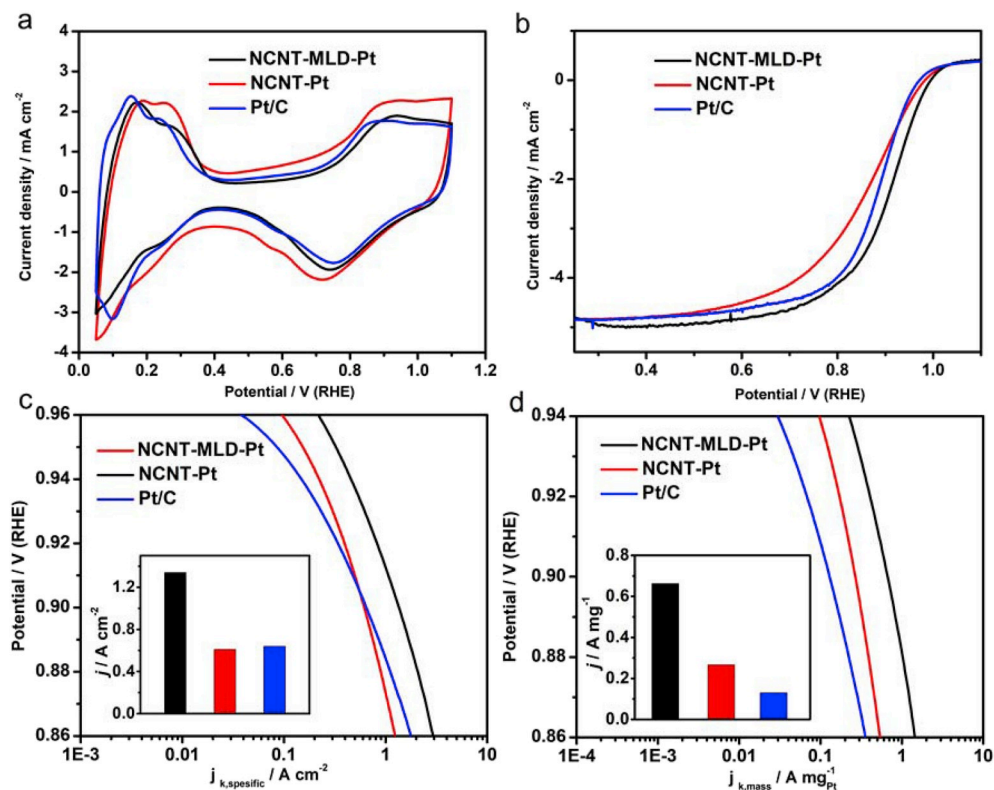


**Fig. 3.** (a) The CV curves in the potential region from 0.05 to 1.10 V. (b) ORR polarization curves of the NCNT-MLD-Pt catalyst and NCNT-Pt catalyst in comparison with commercial Pt/C catalyst. The current densities were normalized to the geometric area of the RDE ( $0.196 \text{ cm}^2$ ). (c) Specific and (d) mass activities given as kinetic current densities ( $j_k$ ) normalized against the ECSAs of the catalysts and the mass of Pt, respectively.

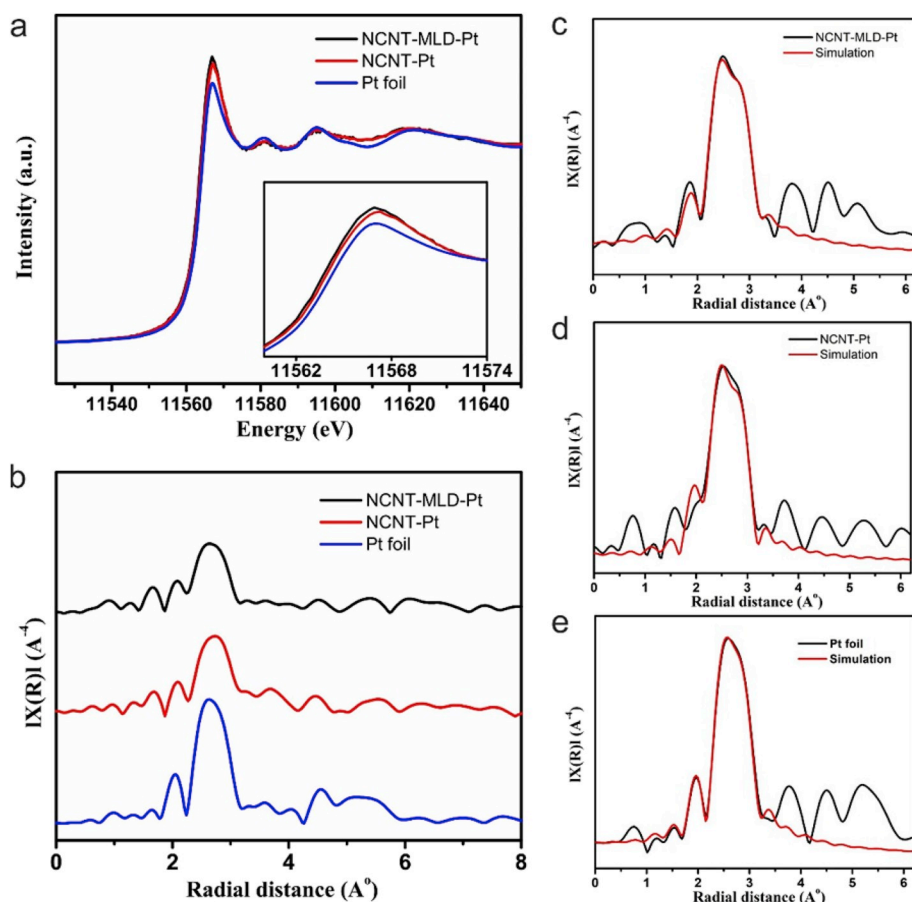


Fig. 4. X-ray absorption studies of the NCNT-MLD-Pt and NCNT-Pt catalysts in comparison with Pt foil. (a) The normalized XANES spectra at Pt L3 edge and (b) The K3-weighted Fourier transform spectra from EXAFS. Inset in (a) shows the enlarged spectra at Pt L3 edge. (c–e) EXAFS fitting in R-space for the samples: NCNT-MLD-Pt, NCNT-Pt and Pt foil.

Table 1  
XAS analysis results for the three ALD samples and reference samples.

Sample	Pt L <sub>3</sub> edge WL		Path	Coordination Number	Bond Length/Å	$\Delta^2/10^{-3} \text{Å}^2$
	E <sub>0</sub> (eV)	E <sub>Peak</sub> (eV)				
Pt foil	11564	11566.6	Pt–Pt	12	2.76	4.7 (0.6)
NCNT-Pt	11563.9	11567.3	Pt–Pt	6.05 (0.57)	2.70	4.1 (0.8)
NCNT-MLD-Pt	11563.4	11566.9	Pt–Pt	5.82 (0.48)	2.63	4.0 (0.5)

is shortened by the deposition of Pt on the MLD-derived NCNT. It has been reported that Pt on different substrates might exhibit significantly different performance [33,34]. For example, Jia and co-workers reported that the shorter Pt–Pt bond distance in the Pt/NbO<sub>x</sub>/C systems could effectively enhance their ORR activity [33]. In our case, the Pt NPs on the TMA-GLY MLD derived carbon interlayer showed shorter Pt–Pt bond distance, compared to Pt on NCNTs. This result indicated that, with the electron transfer from Pt to substrates, the Pt electronic structure was tuned by the MLD interlayer. Accordingly, we speculated that the enhanced ORR activity of NCNT-MLD-Pt was attributed to the shorter Pt–Pt bond distance by the deposition of Pt on the TMA-GLY MLD-derived carbon.

In addition to the ORR activity, we carried out an accelerated durability test (ADT) to evaluate the long-term stability of the NCNT-MLD-Pt catalysts. The test was conducted by applying a cyclic potential sweep between 0.60 and 1.10 V at a sweep rate of 100 mV/s in an O<sub>2</sub>-saturated 0.1 M HClO<sub>4</sub> solution at room temperature. Compared to the NCNT-Pt catalyst, the durability of NCNT-MLD-Pt was significantly enhanced, as shown in Fig. 5, S5 and S6. The ECSAs of NCNT-MLD-Pt was 42.6 m<sup>2</sup>/g<sub>Pt</sub> and 34.0 m<sup>2</sup>/g<sub>Pt</sub> after 10,000 and 20,000 cycles, which only dropped by 14% and 31% compared to the initial ECSA (49.3 m<sup>2</sup>/g<sub>Pt</sub>); while the ECSA of NCNT-Pt dropped by 30% and 48% after 10,000

and 20,000 cycles (Fig. 5a). At 0.9 V<sub>RHE</sub>, the mass activity of the NCNT-MLD-Pt catalyst dropped by 11% and 20%, respectively, after 10,000 and 20,000 cycles; while the mass activity of the NCNT-Pt dropped by 33% and 45%, respectively, after 10,000 and 20,000 cycles (Fig. 5d). The result shows that the changes of ORR mass activity during the durability test corresponded well to the variations in specific surface area. In the case of the NCNT-Pt, its rapidly diminished ECSA and mass activity could be attributed to the Ostwald ripening effect, agglomeration and detachment of the Pt NPs from NCNT during repeated cycles of ORR. The morphology changes of the NCNT-Pt after ADT were examined by TEM. After ADT, the size of the Pt NPs in the NCNT-Pt increased from 5 nm to 10 nm (Fig. S7), indicating that serious ripening or aggregation of the Pt NPs occurred during the CV cycling. In contrast, the MLD-derived interlayer provided a porous structure to protect the Pt particles from dissolution and/or agglomeration during the durability test. After ADT, the size of the Pt NPs in the NCNT-MLD-Pt was still around 5.0 nm and underwent almost no change (Fig. S8a and S8b), suggesting that the MLD-interlayer stabilized the Pt NPs during potential cycling. Additionally, EDS mapping profiles for the post-testing sample still display an even distribution of C, Al and Pt elements on the whole NCNT structure, indicating the good stability of the MLD-derived interlayer (Fig. S8c).

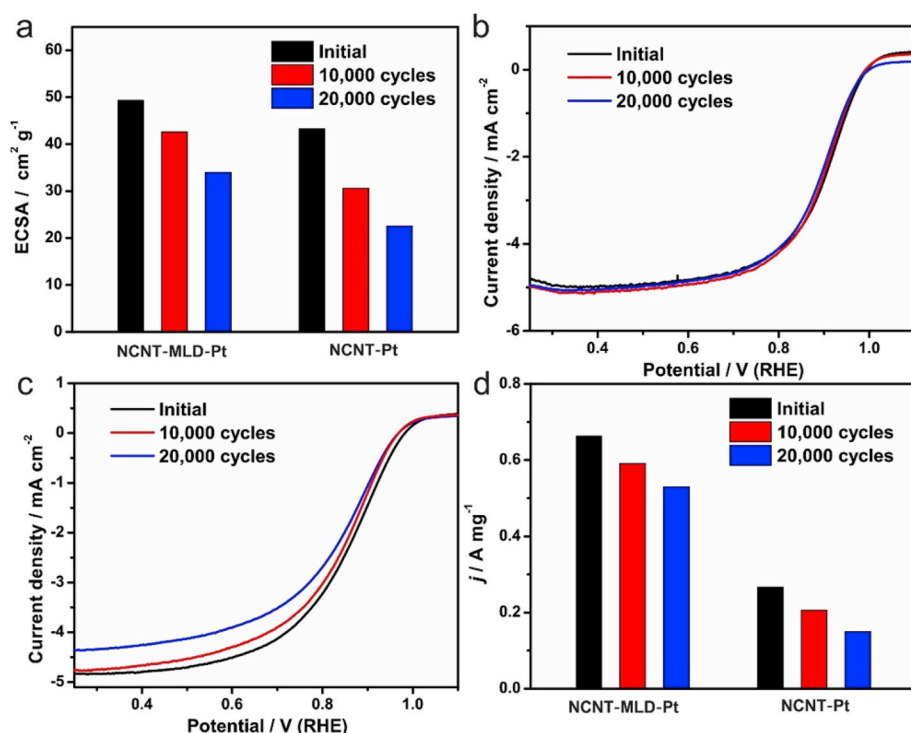


Fig. 5. (a) ECSAs of the NCNT-MLD-Pt and NCNT-Pt catalysts before and after accelerated durability tests. (b) ORR polarization curves for the NCNT-MLD-Pt catalyst after 10,000 and 20,000 cycles accelerated durability tests. (c) ORR polarization curves for the NCNT-Pt catalyst after 10,000 and 20,000 cycles accelerated durability tests. The current densities ( $j$ ) were normalized against the geometric area of the RDE (0.196 cm<sup>2</sup>). (d) Mass activities (0.9 V<sub>RHE</sub>) of the catalysts before and after the accelerated durability tests.

Based on the above results, the MLD derived interlayer on NCNTs is a very effective route to stabilize Pt NPs based on the electrochemical stability tests. It should be pointed out that the MLD cycling number of TMA-GLY coating also played an important role for the Pt performance. To investigate the influence of TMA-GLY MLD cycling numbers on the electrochemical performance of Pt catalysts, 10, 30 and 50 MLD cycle coatings were conducted (Fig. S9). The corresponding annealed samples were used as substrates for the deposition of Pt and the obtained catalysts were named as NCNT-10MLD-Pt, NCNT-30MLD-Pt and NCNT-50MLD-Pt, respectively (Fig. S10). As shown in Fig. S11, we compared the ORR curves of the catalysts with different MLD layers. At 0.9 V<sub>RHE</sub>, the mass activities for the 10, 30, 50 MLD-derived catalysts were calculated to be 0.20, 0.66 and 0.03 A/mg<sub>Pt</sub>. The NCNT-10MLD-Pt catalyst exhibited very similar mass activity compared to NCNT-Pt, indicating that the very thin MLD layer will not influence the activity of Pt. With a relatively thick MLD layer, the NCNT-50MLD-Pt catalyst exhibited a much lower mass activity for ORR, which might due to the relatively low conductivity of thicker MLD-derived interlayer. In addition to controlling the number of MLD cycles, we also tried to directly use the TMA-GLY coating without annealing for the deposition of Pt. The as-prepared catalysts exhibited significantly worse performances due to the poor conductivity of the TMA-GLY MLD layer (Fig. S12). These result further indicated that the annealing step is essential for the fabrication of conductive MLD interlayer.

#### 4. Conclusion

In summary, we fabricated porous TMA-GLY interlayer on NCNTs through a MLD method followed by annealing at high temperature. The Pt catalysts can be successfully deposited onto the MLD-derived surface by ALD. The NCNT-MLD-Pt shows significantly enhanced ORR activity and durability compared to Pt on pure NCNT catalysts. The MLD-derived surface with enriched pores are helpful for anchoring the Pt particles to avoid the agglomeration and detachment. In addition, XAS results show that the deposition of Pt on the MLD-derived interlayer induced the electron transfer from Pt to substrates and reduced the Pt–Pt bond distance, which resulted in the enhanced activity of Pt catalysts. This work provided a novel route for stabilizing Pt catalysts

through the MLD technique.

#### Acknowledgements

This work was supported by Natural Sciences and Engineering Research Council of Canada (NSERC), Canada Research Chair (CRC) Program, Canada Foundation for Innovation (CFI) and the University of Western Ontario.

#### Appendix A. Supplementary data

Supplementary data to this article can be found online at <https://doi.org/10.1016/j.nanoen.2019.03.033>.

#### References

- [1] M.K. Debe, *Nature* 486 (2012) 43–51.
- [2] D. Banham, S. Ye, *ACS Energy Lett.* 2 (2017) 629–638.
- [3] L. Zhang, L.T. Rolling, X. Wang, M. Vara, M. Chi, J. Liu, S.-I. Choi, J. Park, J.A. Herron, Z. Xie, M. Mavrikakis, Y. Xia, *Science* 349 (2015) 412–416.
- [4] C. Chen, Y. Kang, Z. Huo, Z. Zhu, W. Huang, H.L. Xin, J.D. Snyder, D. Li, J.A. Herron, M. Mavrikakis, M. Chi, K.L. More, Y. Li, N.M. Markovic, G.A. Somorjai, P. Yang, V.R. Stamenkovic, *Science* 343 (2014) 1339–1343.
- [5] M. Li, Z. Zhao, T. Cheng, A. Fortunelli, C.-Y. Chen, R. Yu, Q. Zhang, L. Gu, B.V. Merinov, Z. Lin, E. Zhu, T. Yu, Q. Jia, J. Guo, L. Zhang, W.A. Goddard III, Y. Huang, X. Duan, *Science* 354 (2016) 1414–1419.
- [6] P.J. Ferreira, G.J. la O, Y. Shao-Horn, D. Morgan, R. Makharia, S. Kocha, H.A. Gasteiger, *J. Electrochem. Soc.* 152 (2005) A2256–A2271.
- [7] Z.Z. Jiang, Z.B. Wang, Y.Y. Chu, D.M. Gu, G.P. Yin, *Energy Environ. Sci.* 4 (2011) 728–735.
- [8] B.Y. Xia, B. Wang, H.B. Wu, Z. Liu, X. Wang, X.W. Lou, *J. Mater. Chem.* 22 (2012) 16499–16505.
- [9] L. Zhang, L.Y. Wang, C.M.B. Holt, B. Zahiri, Z. Li, K. Malek, T. Navessin, M.H. Eikerling, D. Mitlin, *Energy Environ. Sci.* 5 (2012) 6156–6172.
- [10] S.Y. Huang, P. Ganesan, S. Park, B.N. Popov, *J. Am. Chem. Soc.* 131 (2009) 13898–13899.
- [11] P.M. Arnal, M. Comotti, F. Schuth, *Angew. Chem. Int. Ed.* 45 (2006) 8224–8227.
- [12] P. Lu, C.T. Campbell, Y. Xia, *Nano Lett.* 13 (2013) 4957–4962.
- [13] S.H. Joo, J.Y. Park, C.K. Tsung, Y. Yamada, P.D. Yang, G.A. Somorjai, *Nat. Mater.* 8 (2009) 126–131.
- [14] S. Takenaka, H. Matsumori, K. Nakagawa, H. Matsune, E. Tanabe, M. Kishida, *J. Phys. Chem. C* 111 (2007) 15133–15136.
- [15] S.H. Lee, D.M. Hoffman, A.J. Jacobson, T.R. Lee, *Chem. Mater.* 25 (2013) 4697–4702.

- [16] J. Lu, B. Fu, M.C. Kung, G. Xiao, J.W. Elam, H.H. Kung, P.C. Stair, *Science* 335 (2012) 1205–1208.
- [17] J. Lu, B. Liu, J.P. Greeley, Z. Feng, J.A. Libera, Y. Lei, M.J. Bedzyk, P.C. Stair, J.W. Elam, *Chem. Mater.* 24 (2012) 2047–2055.
- [18] N. Cheng, M.N. Banis, J. Liu, A. Riese, X. Li, R. Li, S. Ye, S. Knights, X. Sun, *Adv. Mater.* 27 (2015) 277–281.
- [19] A.A. Dameron, D. Seghete, B.B. Burton, S.D. Davidson, A.S. Cavanagh, J.A. Bertrand, S.M. George, *Chem. Mater.* 20 (2008) 3315–3326.
- [20] Y. Zhao, X. Sun, *ACS Energy Lett.* 3 (2018) 899–914.
- [21] Q. Peng, B. Gong, R.M. VanGundy, G.N. Parsons, *Chem. Mater.* 21 (2009) 820–830.
- [22] A.I. Abdulagatov, R.A. Hall, J.L. Sutherland, B.H. Lee, A.S. Cavanagh, S.M. George, *Chem. Mater.* 24 (2012) 2854–2863.
- [23] B.H. Lee, B. Yoon, A.I. Abdulagatov, R.A. Hall, S.M. George, *Adv. Funct. Mater.* 23 (2012) 532–546.
- [24] X. Li, A. Lushington, Q. Sun, W. Xiao, J. Liu, B. Wang, Y. Ye, K. Nie, Y. Hu, Q. Xiao, R. Li, J. Guo, T.-K. Sham, X. Sun, *Nano Lett.* 16 (2016) 3545–3549.
- [25] Y. Zhao, L.V. Goncharova, Q. Zhang, P. Kaghazchi, Q. Sun, A. Lushington, B. Wang, R. Li, X. Sun, *Nano Lett.* 17 (2017) 5653–5659.
- [26] X. Liang, J. Li, M. Yu, C.N. McMurray, J.L. Falconer, A.W. Weimer, *ACS Catal.* 1 (2011) 1162–1165.
- [27] Z. Shang, R.L. Patel, B.W. Evanko, X. Liang, *Chem. Commun.* 49 (2013) 10067–10069.
- [28] L.G. Bulusheva, A.V. Okotrub, A.G. Kurennya, H. Zhang, H. Zhang, X. Chen, H. Song, *Carbon* 49 (2011) 4013–4023.
- [29] H.A. Gasteiger, S.S. Kocha, B. Sompalli, F.T. Wagner, *Appl. Catal., B* 56 (2005) 9–35.
- [30] S. Sun, G. Zhang, N. Gauquelin, N. Chen, J. Zhou, S. Yang, W. Chen, X. Meng, D. Geng, M. Banis, R. Li, S. Ye, S. Knights, G. Botton, T.-K. Sham, X. Sun, *Sci. Rep.* 3 (2013) 1775.
- [31] N. Cheng, S. Stambula, D. Wang, M. Banis, J. Liu, A. Riese, B. Xiao, R. Li, T.-K. Sham, L. Liu, G. Botton, X. Sun, *Nat. Commun.* 7 (2016) 13638.
- [32] P. Hu, Z. Huang, Z. Amghouz, M. Makkee, F. Xu, F. Kapteijn, A. Dikhtiarenko, Y. Chen, X. Gu, X. Tang, *Angew. Chem. Int. Ed.* 53 (2014) 3418–3421.
- [33] Q. Jia, W. Liang, M.K. Bates, P. Mani, W. Lee, S. Mukerjee, *ACS Nano* 9 (2015) 387–400.
- [34] Q. Jia, S. Ghoshal, J. Li, W. Liang, G. Meng, H. Che, S. Zhang, Z.-F. Ma, S. Mukerjee, *J. Am. Chem. Soc.* 139 (2017) 7893–7903.



**Dr. Lei Zhang** received his BS degree in Chemistry (2008) and PhD degree in Nanomaterial Chemistry (2014) from Xiamen University with Prof. Zhaoxiong Xie. He was a visiting graduate student at Georgia Institute of Technology in Prof. Younan Xia's group from 2012 to 2014. From 2015 to 2016, he worked as a Postdoc at Collaborative Innovation Center of Chemical Science and Engineering in Tianjin University. He is currently a postdoctoral associate with Prof. Xueliang Sun at Western University. His research interests include the design and synthesis of metal nanomaterials and single atom catalysts for fuel cells and water splitting devices.



**Dr. Yang Zhao** is currently a postdoctoral associate in Prof. Xueliang (Andy) Sun's Group at the University of Western Ontario, Canada. He received his B.S. degree and M.S. degree from Northwestern Polytechnical University (Xi'an, China) in 2011 and 2014, respectively. He obtained his Ph.D. degree in Materials Science and Engineering from University of Western Ontario in 2018. His current research interests focus on atomic layer deposition and molecular layer deposition for energy storage and conversion.



**Dr. Mohammad Norouzi Banis** is a research engineer in Prof. Xueliang (Andy) Sun's group at the University of Western Ontario, Canada. He received his Ph.D. degree in 2013 in Materials Science and Engineering from Western University, on the study of nanostructured low temperature fuel cells and application of x-ray absorption spectroscopy in energy related systems. His current research interests include study of metal ion, metal air and nanocatalysts via in-situ synchrotron-based techniques.



**Keegan Adair** received his BSc in chemistry from the University of British Columbia in 2016. He is currently a PhD candidate in Prof. Xueliang (Andy) Sun's Nanomaterials and Energy Group at the University of Western Ontario, Canada. Keegan has previous experience in the battery industry through internships at companies including E-One Moli Energy and General Motors R&D. His research interests include the design of nanomaterials for lithium metal batteries and nanoscale interfacial coatings for battery applications.



**Dr. Zhongxin Song** is currently a Ph.D. candidate in Prof. Xueliang (Andy) Sun's Group at the University of Western Ontario, Canada. She received her B.S. degree and M.S. degree in Polymer Science and Engineering from Qingdao University of Science and Technology (China) in 2011 and 2014, respectively. Her current research interests focus on design and synthesis of metal nanomaterials, single atom catalyst, and MOFs materials for fuel cells application.



**Dr. Lijun Yang** is a Research Scientist at Ballard Power Systems. She earned her Ph.D. from a joint program between South China University of Technology and Brookhaven National Laboratory. She was a postdoctoral fellow at Institut national de la recherche scientifique EMT at Montreal, Canada. She joined Ballard in 2015 as postdoc and became full timer two years later. She has 10 years of experience in PEMFC catalyst research. Her current work is focus on the application of advanced electro-catalysts in the catalyst layers for PEM fuel cell.



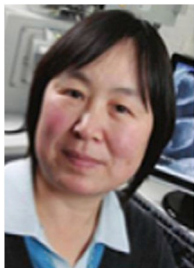
**Dr. Matthew Markiewicz** received his BSc (2006) and PhD in Chemistry (2011) from the University of Alberta with Prof. Steven Bergens, where he worked on catalysts for direct alcohol fuel cells. He then moved to Imperial College London to work with Prof. Anthony Kucernak as a research associate (2012–2017), where he contributed to a broad range of projects that focused on electrodes for REDOX flow batteries and supercapacitors, and fundamental investigations on catalysts for the ORR. He is currently a senior research scientist at Ballard Power Systems, where he continues to focus on catalysts and catalyst layer designs for PEMFCs.



**Junjie Li** is currently a Ph.D. candidate in Prof. Xueliang (Andy) Sun's Group at the University of Western Ontario, Canada. He received his M.S. degree in physical chemistry from University of Science and Technology of China in 2017. Currently, he is working on the synthesis of advanced nanomaterials for fuel cell applications.



**Sizhe Wang** is currently a Ph.D. candidate at School of materials and energy, University of Electronic Science and Technology of China (UESTC), China. At the same time, he is a visiting student in Prof. Xueliang (Andy) Sun's Nanomaterials and Energy Group at University of Western Ontario, Canada. He got his B.S. degree in Electronics Science and Technology from School of Microelectronics and Solid-State Electronics, UESTC, in 2013. Currently, his research interests focus on nanocarbon and advanced functional materials as well as their applications in energy conversion and storage, especially for Na/Li-ion batteries and Li–S batteries.



**Ruying Li** is a research engineer at Prof. Xueliang (Andy) Sun's Nanomaterial and Energy Group at the University of Western Ontario, Canada. She received her Master degree in Material Chemistry under the supervision of Prof. George Thompson in 1999 at University of Manchester, UK, followed by work as a research assistant under the direction of Prof. Keith Mitchell at the University of British Columbia and under the direction of Prof. Jean-Pol Dodelet at l'Institut national de la recherche scientifique (INRS), Canada. Her current research interests are associated with synthesis and characterization of nanomaterials for electrochemical energy storage and conversion.



**Dr. Siyu Ye** is a Fellow of the Canadian Academy of Engineering. He earned his B.S. and Ph.D. from Xiamen University. He was a Postdoctoral Fellow at the University Duisburg and University of Quebec at Montreal, and Principal Research Scientist at Ballard Power Systems. Currently, he is Chief Technology Officer and Board Member at SinoHyKey, Guangzhou, China. He is also an Adjunct Professor at the University of British Columbia, University of Waterloo, South China University of Technology, and South University of Science and Technology of China. Dr. Ye has more than twenty years of fuel cell experience with expertise in electrocatalysis and MEA design. He has over 100 peer-reviewed papers, and over 50 patents and patent applications.



**Prof. Xueliang Sun** is a Canada Research Chair in Development of Nanomaterials for Clean Energy, Fellow of the Royal Society of Canada and Canadian Academy of Engineering and Full Professor at the University of Western Ontario, Canada. Dr. Sun received his Ph.D. in materials chemistry in 1999 from the University of Manchester, UK, which he followed up by working as a postdoctoral fellow at the University of British Columbia, Canada and as a Research Associate at L'Institut National de la Recherche Scientifique (INRS), Canada. His current research interests are focused on advanced materials for electrochemical energy storage and conversion, including electrocatalysis in fuel cells and electrodes in lithium-ion batteries and metal-air battery.